2 and 4) relative to the ν_4 (1374 cm^{-1}) mode. These spectra give a clear-cut comparison of the band intensity and width, since the interfering porphyrin modes are canceled out. It is noted that both the $\nu(^{16}O-^{16}O)$ and $\nu(^{18}O-^{18}O)$ regions are broader for the adamantanone-bound adduct relative to camphor. This is due to the presence of two conformers as discussed in the previous section. However, we emphasize here that the bandwidth of the unresolved features in the ν(O–O) region of the $^{16}O_2$ adduct of the adamantanone-bound enzyme (trace B) is significantly broader than that of the $^{18}O_2$ adduct, though the integrated areas of the positive and negative peaks are identical within experimental error. The observation of selective band broadening of one isotopomer ($^{16}O_2$) can be reasonably ascribed to the enhancement of an internal mode of the bound adamantanone. As can be seen in the Raman spectrum of adamantanone (trace C), several bands occur in this region; in particular, the mode at 1140 cm^{-1} is closely energy-matched with the ν(O–O) frequency. The natural substrate, camphor, however, does not exhibit any band in this region (spectrum not shown), and no evidence of a perturbed spectral pattern is indicated in trace A.

Previously, we had demonstrated such an enhancement of the solvent and solute internal mode via the resonance vibrational coupling in the RR spectra of dioxygen adducts of cobalt porphyrins.[44] In that case, we were able to use isotopically labeled solvents (toluene and chlorobenzene) and various nitrogenous bases to fine-tune the frequencies of ν(O–O) and internal modes so as to systematically study their interactions. It was shown that the enhancement requires a close association of the molecule in question with the bound dioxygen and is critically dependent upon energy matching of the mode with the ν(O–O) stretching frequency. Clearly, these two requirements are satisfied for the dioxygen adduct of adamantanone-bound cytochrome P450cam system, and may be responsible for the observed band broadening in the case of $^{16}O_2$ adduct, although further studies using deuterated adamantanone would be needed to unambiguously confirm such coupling.

Acknowledgment. This work was supported by a grant from the National Institutes of Health (DK35153). The authors are sincerely grateful to Professor S. Sligar of the University of Illinois at Urbana—Champaign for the supply of *P. putida* cell paste.

(44) Kincaid, J. R.; Proniewicz, L. M.; Bajdor, K.; Bruha, A.; Nakamoto, K. *J. Am. Chem. Soc.* **1985**, *107*, 6775-6781.
(45) Benko, B.; Yu, N.-T. *Proc. Natl. Acad. Sci. U.S.A.* **1983**, *80*, 7042-7046.
(46) Bajdor, K.; Oshio, H.; Nakamoto, K. *J. Am. Chem. Soc.* **1984**, *106*, 7273-7274.
(47) (a) Burke, J. M.; Kincaid, J. R.; Peters, S.; Gagne, R. R.; Collman, J. P.; Spiro, T. G. *J. Am. Chem. Soc.* **1978**, *100*, 6083-6087. (b) Walters, M. A.; Spiro, T. G.; Suslick, K. S.; Collman, J. P. *J. Am. Chem. Soc.* **1980**, *102*, 6857-6858. (c) Collman, J. P.; Brauman, J. I.; Halbert, T. R.; Suslick, K. S. *Proc. Natl. Acad. Sci. U.S.A.* **1976**, *73*, 3333-3337.
(48) Nakamoto, K.; Paeng, I. R.; Kuroi, T.; Isobe, T.; Oshio, H. *J. Mol. Struct.* **1988**, *189*, 293-300.
(49) (a) Alben, J. O.; Bare, G. H.; Moh, P. P. In *Biochemical and Clinical Aspects of Hemoglobin Abnormalities*; Caughey, W. S., Caughey, H., Eds.; Academic Press: New York, 1978; pp 607-617. (b) Barlow, C. H.; Maxwell, J. C.; Wallace, W. J.; Caughey, W. S. *Biochem. Biophys. Res. Commun.* **1973**, *55*, 91-95. (c) Maxwell, J. C.; Volpe, J. A.; Barlow, C. H.; Caughey, W. S. *Biochem. Biophys. Res. Commun.* **1974**, *58*, 166-171. (d) Brown, W. E., III; Sutcliffe, J. W.; Pulsinelli, P. D. *Biochemistry* **1983**, *22*, 2914-2923.
(50) Tsubaki, M.; Nagai, K.; Kitagawa, T. *Biochemistry* **1980**, *19*, 379-385.

Structural Models for Covalent Non-Oxidic Glasses. Atomic Distribution and Local Order in Glassy $CdGeP_2$ Studied by ^{31}P and ^{113}Cd MAS and Spin-Echo and $^{31}P-^{113}Cd$ Spin-Echo Double Resonance NMR Spectroscopy

Deanna Franke, Robert Maxwell, David Lathrop, and Hellmut Eckert*

Contribution from the Department of Chemistry, University of California, Santa Barbara, California 93106. *Received October 3, 1990*

Abstract: The structure of glassy $CdGeP_2$ is discussed on the basis of complementary solid-state NMR experiments, including ^{31}P and ^{113}Cd magic-angle spinning (MAS) and spin-echo techniques, as well as $^{31}P-^{113}Cd$ spin-echo double resonance (SEDOR) NMR. Modeling of the dipolar interactions in conjunction with experimental studies on the crystalline model compounds CdP_2 and $CdGeP_2$ reveals the short-range order present in crystalline $CdGeP_2$ is not preserved upon vitrification. In contrast to the crystalline analogue, glassy $CdGeP_2$ contains a substantial fraction of phosphorus–phosphorus bonds, which can be quantitated by means of ^{31}P spin-echo decay data. The analysis reveals that the number of P–P bonds amounts to 55 ± 5% of that expected for a completely random distribution of atoms. The $^{113}Cd-^{31}P$ SEDOR results are qualitatively consistent with this conclusion but suggest a more complete randomization of the Cd atoms. As a consequence of this randomization of atomic occupancies, the number of Cd–P bonds is significantly reduced in the glassy state. The study provides important experimental data for the development of realistic atomic distribution models for covalent non-oxidic glasses.

Introduction

The development of novel materials with properties suitable for applications as low-frequency infrared waveguides still represents a major challenge in materials science. Most of the work carried out so far has concentrated on non-oxidic glasses, based on fluoride, sulfide, and selenide anions.[1] For many of these systems, however, the good optical properties are compromised by major drawbacks such as low glass transition temperatures and a pronounced air and moisture sensitivity. It has been much less widely realized that there exists a whole class of potentially superior materials, based on phosphides and arsenides of main-group and post-transition elements. These glasses are sometimes called the "chalcopyrite glasses", since their prototype compounds exhibiting glass formation, $CdGeAs_2$ and $CdGeP_2$, both crystallize in the chalcopyrite structure. Most importantly from the ap-

(1) Taylor, P. C. *Mater. Res. Soc. Bull.* **1987**, 36. Andriesh, A. M. *J. Non-Cryst. Solids* **1985**, *77/78*, 1219.

0002-7863/91/1513-4822$02.50/0

plications aspect, these glasses are air-stable and have higher glass transition temperatures than non-oxide chalcogenide glasses.

Preparation of $CdGeP_2$ in the glassy state was first reported in 1965,[2] followed by a number of further characterization studies,[3-11] some of which revealed dramatic changes in physicochemical properties upon the crystal-to-glass transition. In these studies, it was noted that glassy $CdGeP_2$ has a higher density than its crystalline counterpart.[3] Such highly unusual behavior suggests that the structures of crystalline and glassy phases are fundamentally different. This indication contrasts sharply with the radial distribution function derived from X-ray diffraction data, which were interpreted in the opposite direction.[6]

Beyond the purpose of resolving this specific disagreement, the present study is also intended to discuss the broader concepts necessary for a structural description of covalent non-oxidic glasses. To date, two well-established structural models are known in the literature: (a) the continuous random network (crn) model and (b) the random close packing (rcp) model. The crn model,[12] applicable to silicate and other oxidic glasses, views the glassy state as a random assembly of well-defined local environments that are analogous to those present in crystalline compounds with the same (or similar) stoichiometries. The lack of long-range periodicity in these glasses arises merely from disorder in the next-nearest-neighbor environments, manifesting itself in a spread of bond angles. The rcp model,[13] on the other hand, is characterized by the complete absence of local order and is generally accepted for the description of amorphous metals. It would be interesting to see if and to which extent these concepts are applicable to covalent non-oxidic glasses.

Initial work carried out in our laboratory on non-oxide chalcogenide glass systems indicates that, contrary to the crn model, the structure of these materials is often characterized by "chemical disorder", i.e., a competition of homoatomic and heteroatomic bond formation.[14] This issue is particularly relevant for the glasses of interest in the current study. Crystalline $CdGeAs_2$ and $CdGeP_2$ are strictly chemically ordered, with As^{3-} and P^{3-} occupying exclusively the anionic sites of the tetragonal chalcopyrite structure. This situation might persist in the glassy state if the crn model is applicable. Alternatively, the rcp model would predict a randomization of anion and cation positions, resulting in an appreciable extent of P–P (or As–As) bonding.

In the present study, we investigate this question by using complementary solid-state NMR techniques. In contrast to the large majority of modern NMR studies of glasses, which rely on chemical shift comparisons for structural information, this study is mostly concerned with the experimental determination and the modeling of internuclear dipole–dipole interactions that influence NMR spectra. In a previous article, we have shown how the measurement of ^{31}P–^{31}P dipolar couplings affords a unique insight into the structure of non-oxidic glasses and allows one to eliminate a variety of possible atomic distribution models.[15] The glass subject to the present study permits us, in principle, to derive structural information from the combined analysis of ^{31}P–^{31}P, ^{113}Cd–^{31}P, and ^{113}Cd–^{113}Cd dipole–dipole couplings. This is done by comparing the experimental results with corresponding lattice calculations from simulated atomic distribution models. Since the approach used here also requires a fundamental understanding of the spin dynamics in these systems, analogous experiments on crystalline model compounds are essential and will be presented here.

Fundamental Concepts and Methodology

Description of Dipolar Interactions. The dipolar interaction in magnetically nondilute systems (as the ones under study here) is most effectively described by a moments analysis. The second moment M_2 for a nucleus dipolarly coupled to surrounding nuclei can be calculated according to van Vleck theory. Two contributions need to be distinguished: "direct" (through-space) dipole–dipole interactions and "indirect" (electron-coupled) dipole–dipole interactions. The *direct* contribution to the dipolar couplings depends on the internuclear distances d_{ij} and can be calculated from an assumed atomic distribution in a straightforward manner:[16] Depending on whether homonuclear or heteronuclear dipole couplings are under discussion, the following expressions have been derived for a polycrystalline material:

$$M_{2d}(\text{homo}) = {}^3/_5(\mu_0/4\pi)^2 I(I+1)\gamma^4\hbar^2 N^{-1}\sum_{i\neq j} d_{ij}^{-6} \quad (1a)$$

$$M_{2d}(\text{hetero}) = \sum_k {}^4/_{15}(\mu_0/4\pi)^2 S(S+1)\gamma_I{}^2\gamma_S{}^2\hbar^2 N^{-1}\sum_S d_{IS}^{-6} \quad (1b)$$

Here γ_I, I, and N are the gyromagnetic ratio, the spin quantum number, and the number of nuclei under observation, and γ_S and S are the gyromagnetic ratios and spin quantum numbers of the k different types of nonresonant nuclei generating dipolar fields at the sites of the observed nuclei. For a discussion of homonuclear interactions only, eq 1a is appropriate if these interactions dominate the rate of the free induction decay (and concomitantly the width of the line shape). If this condition obtains, the line broadening is termed "homogeneous". Equation 1b applies to heteronuclear couplings but is also the appropriate one to use (with $\gamma_I = \gamma_S$ and $I = S$) for homonuclear interactions if other mechanisms such as the chemical shift anisotropy or chemical shift distribution effects are dominant. In such a case, the quantum-mechanical ("flip-flop") term in the dipolar Hamiltonian does not contribute to the dipolar interaction, resulting in the smaller prefactor ($^4/_{15}$). This situation corresponds to the case of "inhomogeneous line broadening". As previously discussed, it is often found to be present in glasses.[17]

The indirect contribution to the dipolar second moment depends on the magnitude of the indirect spin–spin coupling tensor components. Since these tensor components cannot be calculated from first principles from an assumed structure, the presence of strong indirect spin–spin couplings poses a significant limitation to a distance distribution analysis using eq 1a,b. In the present study, it will be assumed that the indirect contributions to ^{31}P–^{31}P and ^{113}Cd–^{31}P interactions are significantly weaker than their direct counterparts, and experimental support for this assumption will be given. In contrast, this assumption is not reasonable for ^{113}Cd–^{113}Cd interactions, since it is well-known that indirect interactions become quite important for heavier nuclei.[18]

Measurement of Homonuclear ^{31}P–^{31}P and ^{113}Cd–^{113}Cd Interactions. As previously described, homonuclear dipole couplings can be selectively measured with use of a simple 90°-t_1-180° spin-echo technique.[19-22] At sufficiently short times, the 180°

(2) Vaipolin, A. A.; Osmanov, E. O.; Rud, Yu. V. *Sov. Phys. – Solid State (Engl. Transl.)* **1966**, *7*, 1833. Vaipolin, A. A.; Goryunova, N. A.; Osmanov, E. O.; Rud, Yu. V. *Dokl. Akad. Nauk SSSR* **1965**, *160*, 633.
(3) Baidakov, L. A.; Kouzova, N. I.; Osmanov, E. O. *Zh. Prikl. Khim. (Leningrad)* **1973**, *46*, 28.
(4) Borshevskii, A. S.; Goryunova, N. A.; Kesamanly, F. P.; Nasledov, D. N. *Phys. Status Solidi* **1967**, *21*, 9.
(5) Goryunova, N. A.; Ryvkin, S. M.; Shpenikov, G. P.; Tichina, I. I.; Fedotov, V. G. *Phys. Status Solidi* **1968**, *28*, 489.
(6) Grigorovici, R.; Manaila, R.; Vaipolin, A. A. *Acta Crystallogr. B* **1968**, *24*, 535.
(7) Goryunova, N. A.; Kuzmenko, G. S.; Mamedov, B. K.; Osmanov, E. O. *Phys. Status Solidi A* **1971**, *8*, 383.
(8) Goryunova, N. A.; Kuzmenko, G. S.; Osmanov, E. O. *Mater. Sci. Eng.* **1971**, *7*, 54.
(9) Borchevskii, A. S.; Kotsyruba, E. S. *Fiz. Khim. Stekla* **1976**, *2*, 365.
(10) Gusatinskii, A. N.; Bunin, M. A.; Blokhin, M. A. *Dokl. Akad. Nauk SSSR* **1977**, *233*, 342.
(11) Akopyan, R. A.; Dovletov, K. O.; Mamedov, B. K. *Izv. Akad. Nauk SSSR, Neorg. Mater.* **1981**, *17*, 1736.
(12) Zachariasen, W. W. *J. Am. Ceram. Soc.* **1932**, *54*, 3841.
(13) Cargill, G. S. *J. Appl. Phys.* **1970**, *41*, 2248; Cohen, M. H.; Turnbull, D. *Nature* **1964**, *203*, 964.
(14) Eckert, H. *Angew. Chem., Adv. Mater.* **1989**, *101*, 1763.
(15) Lathrop, D.; Eckert, H. *J. Am. Chem. Soc.* **1989**, *111*, 3536.
(16) Van Vleck, J. H. *Phys. Rev.* **1948**, *74*, 1168.
(17) Duncan, T. M.; Douglass, D. C.; Csencsits, R.; Walker, K. L. *J. Appl. Phys.* **1986**, *60*, 130. Douglass, D. C.; Duncan, T. M.; Walker, K. L.; Csencsits, R. *J. Appl. Phys.* **1985**, *58*, 197.
(18) Bloembergen, N.; Rowland, T. J. *Phys. Rev.* **1955**, *97*, 1679.
(19) Engelsberg, M.; Norberg, R. E. *Phys. Rev.* **1972**, *B5*, 3395.

pulse refocuses interactions linear in I_z, i.e., chemical shift anisotropy and distribution effects, and heterodipolar ^{113}Cd–^{31}P interactions. The height of the spin-echo thus formed at the time $2t_1$ decreases with increasing evolution time $2t_1$, because homonuclear (^{31}P–^{31}P and ^{113}Cd–^{113}Cd) interactions are not refocused. For multiple interactions (as in the present case), the decay of the echo height $I(2t_1)$ can often be approximated as a Gaussian:

$$I(2t_1)/I(0) = \exp\{-M_{2d}(2t_1)^2/2\} \quad (2)$$

Thus, the homonuclear dipolar second moment M_{2d} can be determined by spin-echo experiments with systematic incrementation of the evolution time $2t_1$ from the semilogarithmic plot defined by eq 2. This value is then to be compared with the average M_{2d} value computed for the P (or Cd) atoms of the simulated structure.

It is important to note that the assumption of complete refocusing of chemical shift terms (and hence the applicability of eq 2) is valid only for short evolution times t_1. This is a consequence of the fact that, during t_1, the density matrix evolves under the combined influence of the dipolar Hamiltonian ($\sim 3I_{z1}I_{z2} - I_1I_2$) and the chemical shift Hamiltonian ($\sim I_z$), which do not commute. On the other hand, a large chemical shift distribution will tend to quench the spin flip-flop transitions, allowing the dipolar Hamiltonian to be truncated to the commuting $I_{z1}I_{z2}$ term. Since it is difficult to estimate the error in this assumption on theoretical grounds, this question will be addressed experimentally in the present study, by using a variety of crystalline model compounds with comparable spin dynamics. The results of these experiments are useful to give an estimate on the valid time domain within which the spin-echo decay can be considered to arise purely from dipolar interactions.

It has been pointed out previously that, for a random distribution of nuclei over a cubic lattice, the spin-echo decay will display marked deviations from Gaussian character in the limit of high dilution.[23] This is so because the randomness produces a large spread of ^{31}P–^{31}P internuclear lattice sums and corresponding second moments. Therefore, all of the various observed ^{31}P nuclei decay in $2t_1$ at widely different individual rates. The resulting overall spin-echo decay can then be viewed as a superposition of Gaussian decay curves:

$$I(2t_1)/I(0) = \sum \exp\{-M_{2d}(2t_1)^2/2\} \quad (3)$$

The foregoing discussion applies equally to ^{113}Cd–^{113}Cd interactions, although we expect a distance distribution analysis from ^{113}Cd spin-echo NMR to be invalidated by indirect dipole–dipole couplings.

Measurement of Heterodipolar ^{31}P–^{113}Cd Interactions. The development of selective NMR approaches toward the determination of heterodipolar interactions in pairs of isolated heteronuclear spins has recently attracted great interest. All of these techniques, known as "spin-echo double resonance" (SEDOR),[24-27] "rotational-echo double resonance" (REDOR),[28] and "rotary resonance recoupling" (RRR)[29] have in common that they convert a heterodipolar coupling, which usually behaves as a source of inhomogeneous line broadening, into a source of homogeneous broadening, whose effect in the time domain is then no longer refocusable by either 180° pulses or MAS. Consequently, the transverse magnetization decay during the experimentally defined evolution time for which this heterodipolar interaction is active can be used as a source of structural information.

Since MAS does not result in any rotational echoes or line narrowing for either the ^{113}Cd or the ^{31}P resonances in glassy $CdGeP_2$, SEDOR appears to be the most suitable technique for the present problem. Physical principles and a few applications of the SEDOR experiment have been described previously.[24-27] In our present application, we conduct a ^{113}Cd spin-echo experiment with simultaneous 180° pulse irradiation of the ^{31}P resonance at the time of the ^{113}Cd refocusing pulse. In principle, the ^{113}Cd SEDOR decay is then governed by the combined effect of Cd–Cd and Cd–P interactions:

$$I(2t_1)/I_0 = \sum \exp\{-(2t_1)^2M_{2Cd\text{-}Cd}/2\} \exp\{-(2t_1)^2M_{2Cd\text{-}P}/2\} \quad (4)$$

As will be illustrated later with experimental results, the M_{2d} relating to the ^{113}Cd–^{113}Cd interaction is usually not predictable from eq 1b. Thus, when the determination of the ^{113}Cd–^{31}P interaction is of interest, it is more practical to analyze and simulate the experimental SEDOR decay data according to

$$I(2t_1)/I_0 = F(2t_1)/F_0 \sum \exp\{-(2t_1)^2M_{2Cd\text{-}P}/2\} \quad (5)$$

where $F(2t_1)/F_0$ is the ^{113}Cd spin-echo decay function measured in the absence of the ^{31}P pulse.

It is important to realize that SEDOR results can be seriously affected by systematic experimental errors if the 180° (^{31}P) pulse is imperfect and/or applied off resonance. In that case, only a fraction of ^{31}P spins are flipped and hence the ^{113}Cd spin-echo decays more slowly with $2t_1$ than expected. This situation has been discussed by previous workers.[26,27] To account for this experimental artifact, eq 5 then has to be replaced by

$$I(2t_1)/I_0 = F(2t_1)/F_0[(1 - a) + a\sum \exp\{-(2t_1)^2M_{2Cd\text{-}P}/2\}] \quad (6)$$

where a ($0 \le a \le 1$) denotes the degree to which the ^{31}P magnetization is inverted by the 180° pulse. It characterizes the fraction of ^{31}P spins actually flipped by the pulse. For very broad lines and in the absence of spin diffusion, the inversion is incomplete for those nuclei contributing to the off-resonance edges of the wide-line NMR spectrum, resulting in a nonunity value for a.

Experimental Section

Sample Preparation and Characterization. Crystalline $CdGeP_2$ and CdP_2 were prepared from the elements in evacuated (10^{-3} Torr) silica glass ampules with a published procedure.[30] The temperature was increased slowly to 450 °C, kept there overnight, and then increased to 800 °C. After 24 h at this temperature, the samples were cooled slowly (20–60 °C/h) to room temperature. The resting period at 450 °C is crucial in order to avoid too rapid evaporation of phosphorus prior to reaction. Violent explosions and fires (due to elemental phosphorus) resulted if the heating rates were too high. X-ray powder diffraction data confirmed that phase-pure materials were formed. The CdP_2 powder pattern matched the JCPDS file (22-127) for the high-temperature tetragonal phase, which is isostructural with the corresponding zinc compound.[31] No evidence was found for the presence of the orthorhombic low-temperature phase (JCPDS file 23-96).[32]

Several replicate samples of glassy $CdGeP_2$ were synthesized with a similar heating procedure, followed by rapid quenching of the ampules in ice–water. Glass transition temperatures, measured with use of a Du Pont 912 differential scanning calorimeter, ranged from 445 to 450 °C, in accordance with literature results.[9]

Solid-State NMR Studies. Solid-state NMR studies were carried out on a General Electric GN-300 spectrometer equipped with a 2-MHz digitizer. The resonance frequencies were 121.65 and 66.71 MHz for ^{31}P

(20) Boden, N.; Gibb, M.; Levine, Y. K.; Mortimer, M. *J. Magn. Reson.* **1974**, *16*, 471.
(21) Warren, W. W.; Norberg, R. E. *Phys. Rev.* **1967**, *154*, 227.
(22) Mortimer, M.; Moore, E. A.; Apperley, D. C.; Oates, G. *Chem. Phys. Lett.* **1987**, *138*, 209.
(23) Abragam, A. *The Principles of Nuclear Magnetism*; Claredon Press: Oxford, 1983; p 125 (paperback issue).
(24) Makowka, C. D.; Slichter, C. P.; Sinfelt, J. H. *Phys. Rev. Lett.* **1982**, *49*, 379. *Phys. Rev. B* **1985**, *31*, 5663.
(25) Wang, P. K.; Slichter, C. P.; Sinfelt, J. H. *Phys. Rev. Lett.* **1984**, *53*, 82.
(26) Shore, S. E.; Ansermet, J. P.; Slichter, C. P.; Sinfelt, J. H. *Phys. Rev. Lett.* **1987**, *58*, 953.
(27) Boyce, J. B.; Ready, S. E. *Phys. Rev. B* **1988**, *38*, 11008.
(28) Gullion, T.; Schaefer, J. *J. Magn. Reson.* **1989**, *81*, 196.
(29) Oas, T. G.; Levitt, M. H.; Griffin, R. G. *J. Chem. Phys.* **1988**, *89*, 692.
(30) Lazarev, V. B.; Shevchenko, V. J.; Marenkin, S. F.; Magomedgadghiev, G. *J. Cryst. Growth* **1977**, *38*, 275.
(31) White, J. G. *Acta Crystallogr.* **1965**, *18*, 217.
(32) Goodyear, J.; Steigmann, G. A. *Acta Crystallogr.* **1969**, *B25*, 2371.

Table I. ^{31}P and ^{113}Cd Chemical Shift Parameters (ppm) and Calculated and Experimental (in Brackets) Dipolar Second Moments (10^6 rad^2/s^2; Typical Experimental Error ±5%) in Crystalline CdP_2 and $CdGeP_2$[a]

parameter	$CdGeP_2$	CdP_2
	^{113}Cd MAS-NMR	
δ_{11}	225 ± 2	23 ± 3
δ_{22}	236 ± 1	154 ± 3
δ_{33}	250 ± 1	469 ± 3
δ_{iso}	237.1 ± 0.3	215.0 ± 0.3
	^{31}P MAS-NMR	
δ_{11}	−80 ± 3	−268 ± 4, −174 ± 3[d]
δ_{22}	−33 ± 3	−124 ± 4, −89 ± 3
δ_{33}	16 ± 3	41 ± 4, 93 ± 3
δ_{iso}	−32.2 ± 0.5	−117.1 ± 0.5, −56.6 ± 0.5
	Dipolar NMR	
M_2 (^{31}P-^{31}P)	11.2 [33.4][b]	56.8 (67)[c]
M_2 (^{113}Cd-^{113}Cd)	0.047 [0.26]	0.055 (0.6)
M_2 (^{31}P-^{113}Cd)	19.2 [8.2]	17.1 (16.4)

[a] Chemical shift references are 85% H_3PO_4 and liquid $Cd(CH_3)_2$ for ^{31}P and ^{113}Cd, respectively. [b] Values in square brackets are experimental data for *glassy* $CdGeP_2$. No experimental data are reported for the crystalline compound, due to the complications discussed in the text. [c] Values in parentheses denote experimental values on crystalline CdP_2. [d] The two values correspond to the two different sites.

and ^{113}Cd, respectively. For high-speed single-resonance ^{31}P MAS experiments, a 5-mm Doty probe was used (3-μs 90° pulse). ^{113}Cd MAS-NMR studies with ^{31}P decoupling employed a 7-mm doubly broad-band tuned probe from Doty Scientific. Typical 90° pulse lengths were 5–8 μs (^{31}P) and 7–10 μs (^{113}Cd). The ^{31}P decoupling frequency was generated by mixing the pulsed ^1H decoupler output with a local oscillator (PTS 250) and subsequent amplification (Amplifier Research LP 50 and Henry Radio amplifiers) to approximately 200 W. The irradiation frequencies for ^{113}Cd and ^{31}P were carefully adjusted to minimize resonance offset effects. The spin-echo and SEDOR experiments were conducted with the same 7-mm probe. Experiments were carried out with recycle delays ranging from 15 to 120 min, yielding no variations in the results within experimental error. Most experiments were carried out with 1-h recycle delays. Due to excellent signal-to-noise ratio, the ^{31}P spin-echo heights could be measured directly from the graphs, whereas the ^{113}Cd spin-echo heights were obtained by fitting the relatively noisy echoes to a Gaussian function (Lorentzian fits for comparison yielded virtually identical results). I_0, the spin-echo height at zero evolution time, was obtained from a polynomial fit to the experimental data. This value was then used to normalize the data. All experiments were carried out on two independently prepared samples, yielding the same results within experimental error.

Analysis and Simulations of Spin-Echo and SEDOR Decays. To extract dipolar coupling information from the experimental spin-echo and SEDOR decays, two approaches are used here.

(1) To obtain a quick numerical estimate of the dipolar coupling strength, the initial parts of the spin-echo decays (up to ca. 50–70% of the initial value) have been analyzed in terms of a Gaussian decay to yield approximate average second moment values. While this analysis is not very precise, it gives a quick impression regarding strength of the dipolar coupling in comparison with the second moment expected from eq 1b. These comparisons have been included in Table I.

(2) To provide more detailed insights, the experimentally observed spin-echo and SEDOR decays are compared with simulations for assumed atomic distribution models. Figure 1 schematically illustrates the difference between both models tested here.

Model a corresponds to a chemically ordered distribution of P (or Cd) atoms strictly over the destined lattice sites in the chalcopyrite structure. The spin echo decay is assumed to be Gaussian, corresponding to the second moment of crystalline $CdGeP_2$, and scaled in order to account for the slight density difference between crystal and glass.

Model b assumes that the atoms under consideration distribute themselves randomly over all the available sites of a zincblende lattice having the same density as glassy $CdGeP_2$. This model mimicks the rcp distribution. For the placements of the atoms, all the sites present in a cube of 7 × 7 × 7 unit cells are considered. For the modeling of the heteronuclear ^{113}Cd–^{31}P interactions, both species are distributed independently over these sites.

Second moments are then calculated for each individual observe nucleus in the inner 3 × 3 × 3 unit cell area with eq 1b and all distances to other atoms in the entire volume contributing to the dipolar fields under consideration. This is repeated for at least 200 separate volumes at each concentration. Due to the randomness of these simulated structures, the dipolar couplings are characterized by distribution functions of second moments, rather than by singular values. On the basis of such distributions, the homo- and heteronuclear decays of the echo heights $I(2t_1)/I_0$ are calculated as superpositions of individual Gaussian decays according to eqs 3, 5, or 6. In the simulations of the ^{31}P–^{113}Cd SEDOR decay data, the decay contribution due to ^{113}Cd–^{113}Cd interactions was not modeled, but taken into account experimentally by measuring $F(2t_1)/F_0$ in the absence of the ^{31}P 180° pulse. The data were fitted to a polynomial and then used to correct the SEDOR decay function calculated from the atomic distribution model.

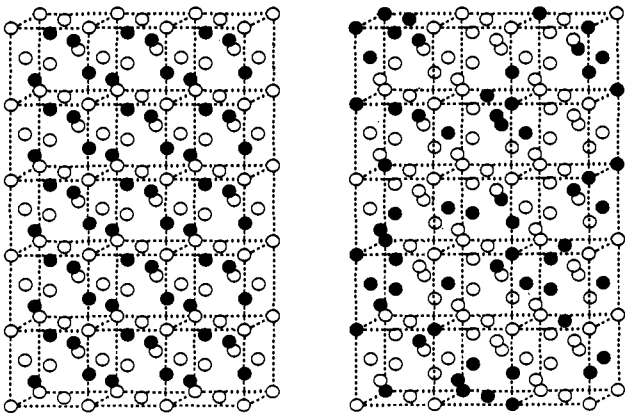

Figure 1. Possible atomic distribution schemes for glassy $CdGeP_2$: (a) chemically ordered structure as present in the crystalline compound; (b) rcp model, random distribution over a cubic lattice (zincblende).

Results

For a discussion of the various NMR experiments carried out in this study, we will briefly review the crystallographic information available for the two model compounds CdP_2 and $CdGeP_2$. The local phosphorus and cadmium environments present in these crystals are summarized in Figure 2.

The structure of crystalline CdP_2 is based on infinite P–P–P zigzag chains with Cd atoms inserted in between.[31] Two crystallographically inequivalent P atoms are present, both of which have highly distorted tetrahedral environments consisting of two P and two Cd atoms. The Cd atoms are coordinated by four phosphorus atoms in a highly distorted tetrahedral arrangement.

The nearest-neighbor environments present in crystalline $CdGeP_2$ are distorted to a substantially lesser degree and approach tetrahedral symmetry.[33] In contrast to CdP_2, the structure of $CdGeP_2$ contains no P–P bonds.

^{31}P and ^{113}Cd MAS-NMR. Figures 3 and 4 compare the ^{31}P and ^{113}Cd MAS-NMR spectra of crystalline CdP_2, $CdGeP_2$, and glassy $CdGeP_2$. The isotropic and anisotropic ^{31}P and ^{113}Cd chemical shift parameters derived from these spectra are summarized in Table I. As expected from the crystal structure, two ^{31}P resonances are observed in CdP_2, with noticeable triplet structure due to scalar $^1J(^{31}P$–$^{31}P)$ spin–spin coupling (Figure 3). The large ^{31}P chemical shift difference between these two sites is surprising in view of the small differences in the nearest-neighbor bond angle distributions. The strong distortions present for both phosphorus sites are reflected by the large anisotropies and asymmetry parameters characterizing the chemical shift tensors. This observation contrasts with the substantially smaller ^{31}P chemical shift anisotropy in crystalline $CdGeP_2$.

The ^{113}Cd MAS-NMR spectra of the model compounds (Figure 4) are again in accord with the expectation from the crystal structures. The chemical shift anisotropy in CdP_2 is substantially larger than in $CdGeP_2$.

The MAS-NMR results obtained for glassy $CdGeP_2$ are included in Figures 3 and 4 to facilitate comparison with the model

(33) Pfister, H. *Acta Crystallogr.* **1958**, *11*, 221.

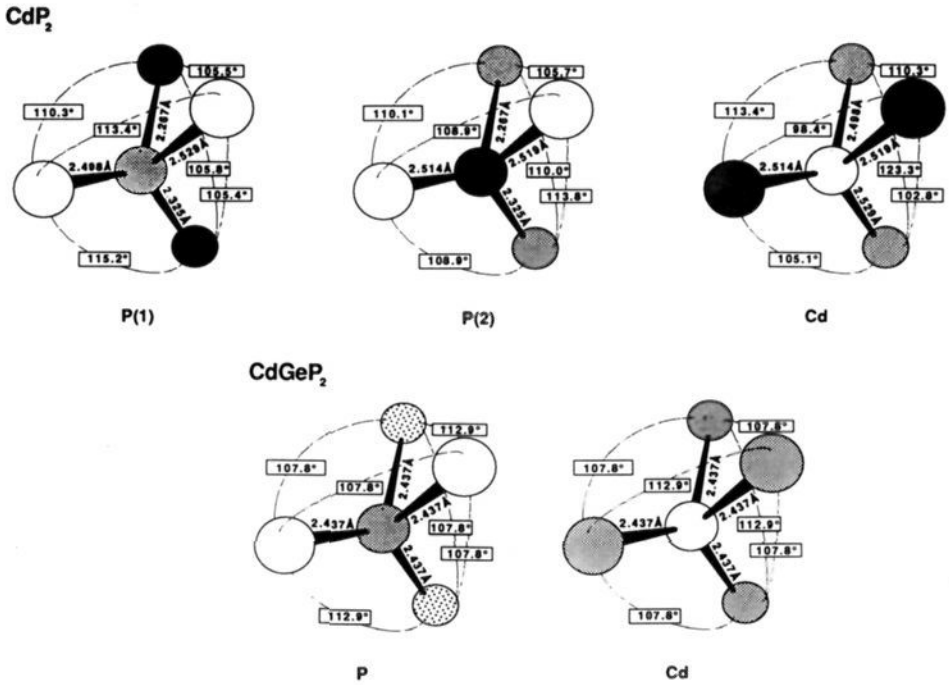

Figure 2. P and Cd short-range order in crystalline $CdGeP_2$ and CdP_2.

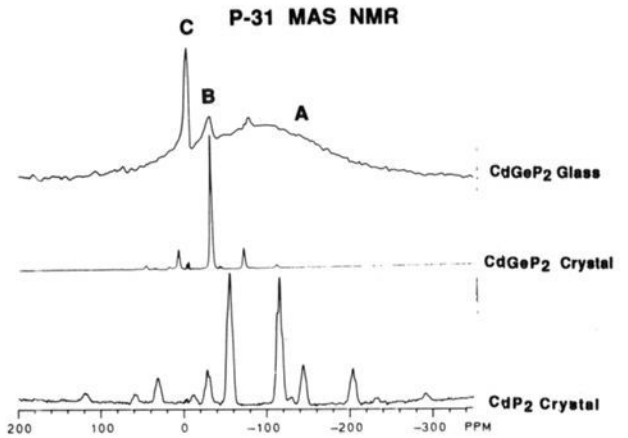

Figure 3. 121.65-MHz ^{31}P MAS-NMR spectra of (a) crystalline CdP_2, spinning speed 9.0 kHz; (b) crystalline $CdGeP_2$, spinning speed 4.8 kHz; and (c) glassy $CdGeP_2$, spinning speed 9.0 kHz. Peaks with weaker intensities are spinning sidebands.

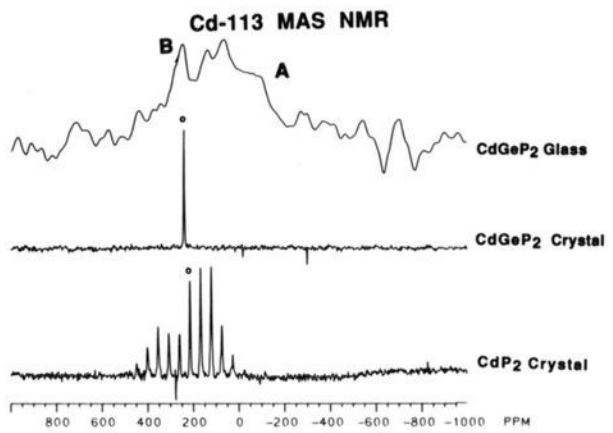

Figure 4. 66.71-MHz ^{113}Cd MAS-NMR spectra of (a) crystalline CdP_2, spinning speed 3.3 kHz; (b) crystalline $CdGeP_2$, spinning speed 4.8 kHz; and (c) glassy $CdGeP_2$, spinning speed 9.0 kHz. The centerbands are indicated by a circle. The spectra on the crystalline compounds were obtained with ^{31}P cw decoupling on resonance.

compounds. The major ^{113}Cd and ^{31}P resonances (resonance "A") are extremely broad and displaced upfield relative to crystalline $CdGeP_2$. In addition, both spectra show minor sharp resonances ("B"), indicating a small amount of crystalline $CdGeP_2$. Furthermore, a sharp feature ("C") is seen in the ^{31}P MAS-NMR spectra around −4 ppm. Closer inspection (with no line broadening prior to FT) reveals that this feature consists of two peaks at −2.5 and −4.5 ppm and a shoulder at −5.5 ppm. These peaks appear consistently in replicate preparations of glassy $CdGeP_2$ and are also present in all crystalline and glassy samples of the system $CdGeP_2$–$CdGeAs_2$,[34] and even in CdP_2. Neither X-ray diffraction nor the ^{113}Cd MAS-NMR spectra show any evidence of a crystalline impurity phase other than a trace of crystalline $CdGeP_2$. Thus, the possibility that these resonances are intrinsic to these systems cannot be ruled out. Similar intrinsic resonances have been observed in crystalline $ZnSnP_2$ and attributed to site disordering.[35] We note that the ^{31}P MAS-NMR spectrum greatly overemphasizes the area fraction of these sharp resonances, since a large fraction of the broad majority signal is not detected due to the rapid decay of the corresponding FID during the dead time (10 μs) of the spectrometer.

Figures 5 and 6 demonstrate that ^{31}P decoupling greatly aids the spectroscopic resolution achievable in the ^{113}Cd MAS spectra of the crystalline model compounds. This improved resolution is particularly useful in the case of crystalline $CdGeP_2$, allowing determination of the small chemical shift anisotropy from MAS sideband patterns obtained at very low spinning speeds. Although dramatic line narrowing is also observed in the CdP_2 case, the resulting effect is most likely incomplete here because the ^{31}P chemical shift anisotropy (Hz) is much larger than the spinning speed employed. As a consequence, only a fraction of the observed nuclei is efficiently decoupled at any given phase of the rotor cycle.

^{31}P Spin-Echo NMR. Figure 7 compares the ^{31}P spin-echo decays observed for various crystalline model compounds. These model compounds were studied because they have dipole–dipole coupling strengths and chemical shift spreads (due to inequivalent sites and shift anisotropies) that are comparable to those in glassy $CdGeP_2$. The experimental data are compared with simulations

(34) Franke, D. R.; Eckert, H. *J. Phys. Chem.* **1991**, *95*, 331.
(35) Ryan, M. A.; Peterson, M. W.; Williamson, D. L.; Frey, J. S.; Maciel, G. E.; Parkinson, B. A. *J. Mater. Soc.* **1987**, *2*, 528.

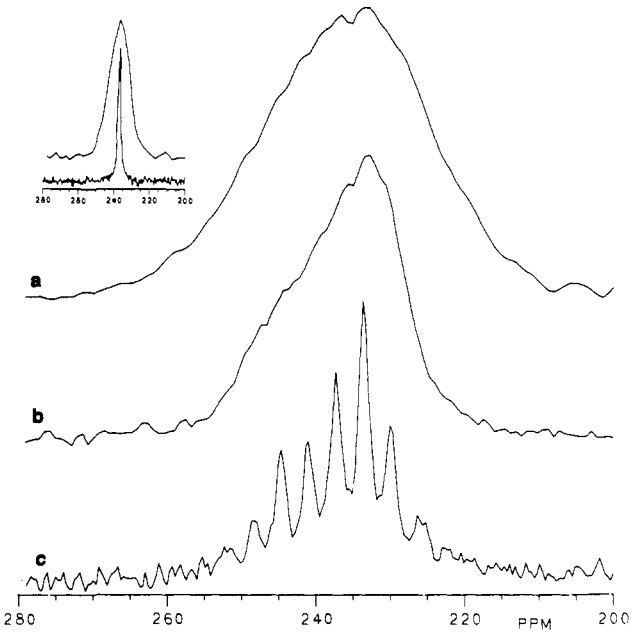

Figure 5. 66.70-MHz ^{113}Cd wide-line and MAS NMR spectra of crystalline $CdGeP_2$, with and without ^{31}P decoupling: (a) ^{113}Cd single-resonance MAS-NMR spectrum (spinning speed 0.25 kHz), this spectrum is identical with the single-resonance NMR spectrum of the stationary sample; (b) $\{^{31}P\}^{113}Cd$ double-resonance spectrum (stationary sample); (c) $\{^{31}P\}^{113}Cd$ double-resonance MAS-NMR spectrum (spinning speed 0.25 kHz). The inset shows a comparison of single- and double-resonance ^{113}Cd NMR spectra (top and bottom, respectively) at a spinning speed of 5 kHz.

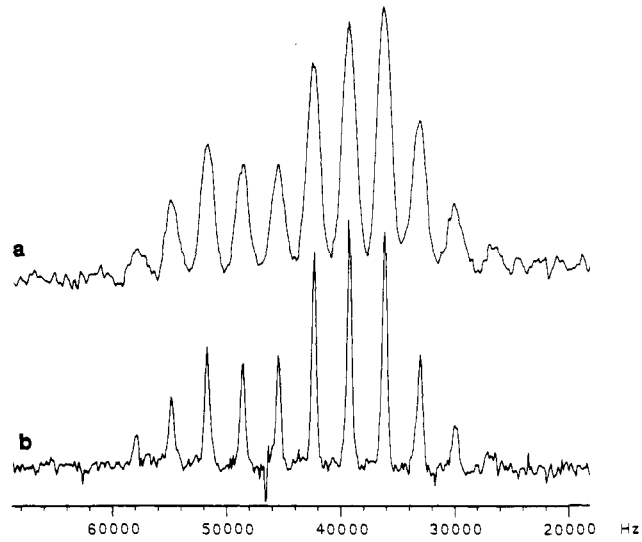

Figure 6. 66.71-MHz ^{113}Cd MAS-NMR spectrum of crystalline CdP_2, (b) with and (a) without ^{31}P decoupling. Spinning speed is 3.3 kHz.

assuming purely dipolar Gaussian decays (eq 2), with M_{2d} values calculated via eq 1b, assuming only direct dipole–dipole couplings. Figure 8 shows the corresponding comparison between experimental data and simulations for glassy $CdGeP_2$, considering a chemically ordered structure analogous to that of crystalline $CdGeP_2$, a random distribution of the P atoms over all the lattice sites, and an additive superposition of both. Table I includes average experimental second moments, as determined from the Gaussian analysis of the initial part of the spin-echo decay.

^{113}Cd Spin-Echo NMR. Figure 9 shows the results of the ^{113}Cd spin-echo experiment on crystalline CdP_2, contrasted with the corresponding calculated decay from the crystal structure. Note that the decay is significantly faster than expected from eq 1b.

Figure 10 shows the ^{113}Cd spin-echo results obtained on glassy $CdGeP_2$. The data are compared to the corresponding calculated decay expected for the chemically ordered $CdGeP_2$ (chalcopyrite) structure and a random distribution, respectively. Although the agreement seems quite good in the latter case, this result may be accidental only, in view of the striking discrepancy seen in Figure 9 for CdP_2. Table I includes average second moments derived from the Gaussian analysis of the initial part of the experimental spin-echo decay.

^{113}Cd-^{31}P SEDOR NMR. Figure 11 shows ^{113}Cd–^{31}P spin-echo double resonance NMR results on the model compound CdP_2. The experimental data are compared with the simulation based on the calculable ^{31}P–^{113}Cd interaction in the crystal structure of this compound. Simulations with various values for the ^{31}P flipping efficiency a are included, by using eq 6. While the assumption $a = 1.0$ yields reasonably good agreement, Figure 11 demonstrates that a description with $a = 0.9 \pm 0.1$ may be more realistic. Figures 12 and 13 contrast the experimental SEDOR data on glassy $CdGeP_2$ with the corresponding responses calculated for crystalline $CdGeP_2$ and the random distribution, respectively, for three assumed values of ^{31}P spin inversion efficiencies a. To illustrate the achievable precision, results from two independent data sets are shown. Table I also includes average second moments as derived from the Gaussian analysis of the initial part of the SEDOR decay.

Discussion

The success of the experimental dipolar spin-echo approaches used here for the deduction of atomic distribution models for glassy $CdGeP_2$ rests with two important questions: (a) Do the simple spin-echo sequences used here produce sufficiently accurate dipolar second moments in these systems and (b) can such experimental second moments be solely attributed to direct dipole–dipole couplings, calculable from eq 1b? With regard to the first question, we have to be concerned with the valid time domain, during which the refocusing of chemical shifts can be considered complete, so that the decay is entirely due to dipolar interactions. With regard to the second issue, we have to be concerned about indirect ^{31}P–^{31}P, ^{113}Cd–^{113}Cd, or ^{31}P–^{113}Cd interactions and homogeneous contributions to the ^{31}P–^{31}P dipolar interactions (due to ^{31}P spin flip-flop processes) that would accelerate the dipolar decays in the ^{31}P, ^{113}Cd, and ^{31}P–^{113}Cd spin-echo experiments, respectively.

To address these questions, we will at first discuss the spin dynamics in the crystalline model compounds, especially CdP_2 and $CdGeP_2$, as inferred from MAS and dipolar spin echo NMR in conjunction with the crystallographic information available. Following this discussion, we will offer possible structural conclusions about glassy $CdGeP_2$.

Spin Dynamics in Crystalline CdP_2. While Figure 7 shows excellent agreement between experiments and simulations for crystalline model compounds, it is noticeable that the experimental ^{31}P spin-echo decay of CdP_2 is slightly more rapid than predicted, resulting in a second moment that is ca. 20% higher than that based on eq 1b. The broad lines seen in the ^{113}Cd MAS-NMR spectrum of CdP_2 and the striking effect of ^{31}P decoupling illustrate that the ^{31}P–^{113}Cd dipolar coupling is partly homogeneous in character, i.e., ^{31}P spin flip-flop processes do occur on the time scale of the MAS rotation period and hence interfere with the refocusing process. For comparison, the ^{113}Cd MAS-NMR spectra of $CdAs_2$ and $CdGeAs_2$ are significantly sharper. In these compounds, the ^{75}As spins are effectively self-decoupled by fast quadrupolar relaxation, and hence the ^{113}Cd–^{75}As dipolar interactions do not contribute significantly to the ^{113}Cd MAS-NMR line width.[34]

The effect of ^{31}P flip-flops can also account for the ^{113}Cd spin-echo decay data, which show a large discrepancy to the simulation. It is well-known that, in a spin-echo experiment executed on spins I coupled to heteronuclei S, the heterodipolar I–S interactions are not completely refocusable by the 180° pulse if, due to flip-flop processes, the S spin states change on the time scale of the experiment.[36] A phenomenological theory for this effect has been formulated by Reimer and Duncan.[36] For the

(36) Reimer, J. A.; Duncan, T. M. *Phys. Rev. B* **1983**, *27*, 4895.

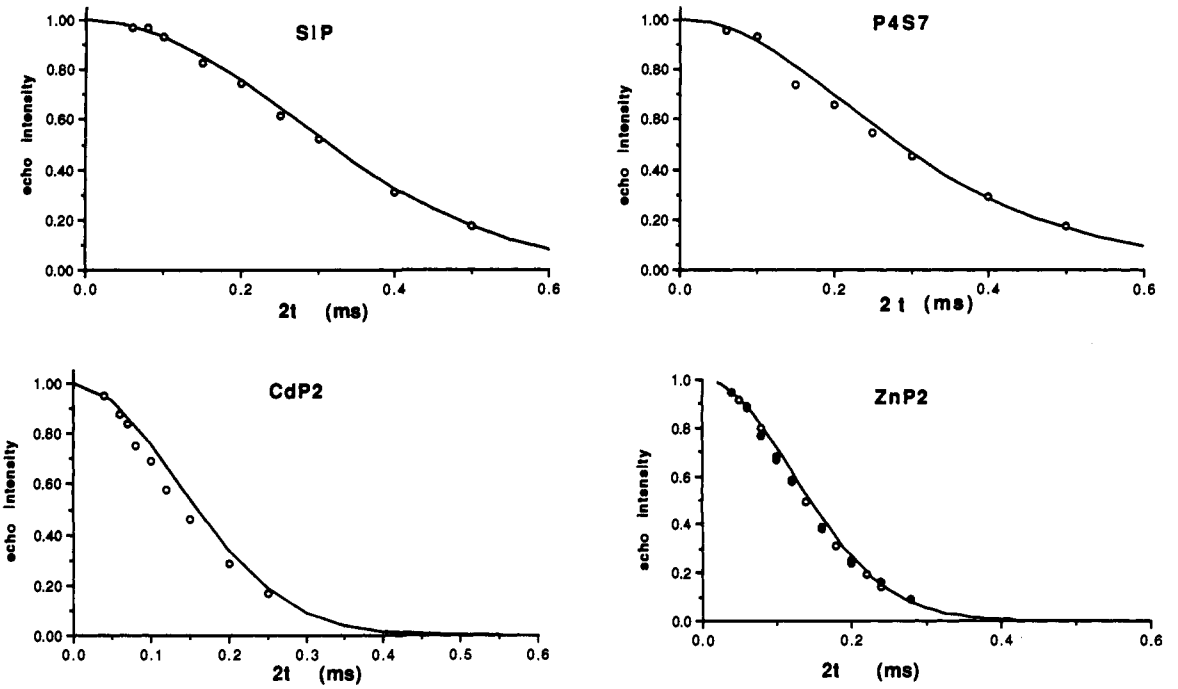

Figure 7. ^{31}P spin-echo decay in crystalline model compounds.[39] Circles show experimental spin-echo heights, whereas the solid curves show the spin-echo decay intensity calculated from eq 2, assuming that the decay is only due to direct ^{31}P–^{31}P spin–spin couplings, calculated from the crystal structures with eq 1b. For ZnP_2, two separate experimental data sets are shown.

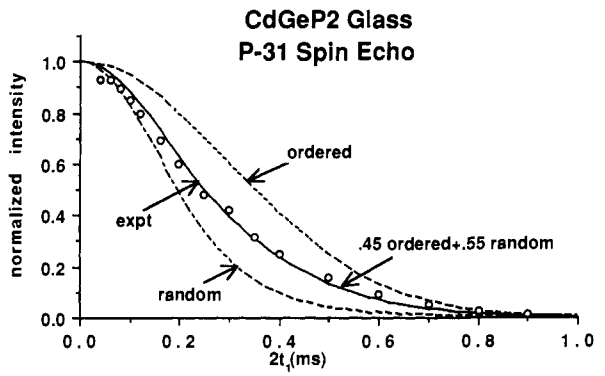

Figure 8. ^{31}P spin-echo decay in glassy $CdGeP_2$ compared to the following simulations: (a) crystalline $CdGeP_2$, (b) random distribution of P atoms over all sites of the chalcopyrite structure, (c) a 45:55% distribution of both situations.

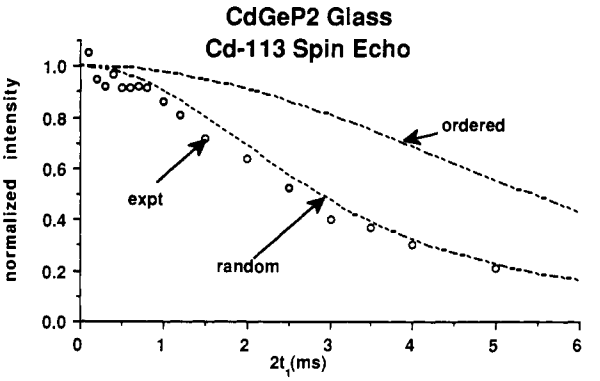

Figure 10. ^{113}Cd spin-echo decay in glassy $CdGeP_2$ compared to the following simulations: (a) crystalline $CdGeP_2$, (b) random distribution of P atoms over all sites of the chalcopyrite structure. The good agreement seen in the random distribution is possibly coincidental.

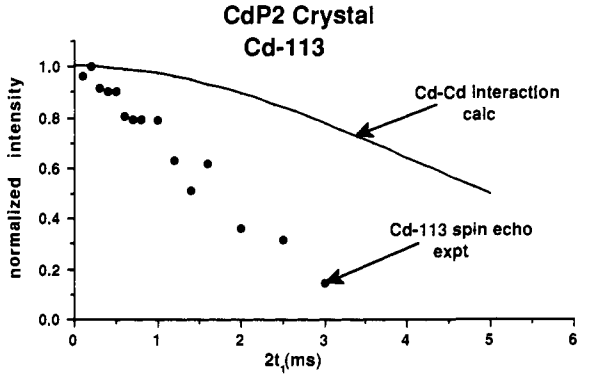

Figure 9. ^{113}Cd spin-echo decay in crystalline CdP_2. The solid curve corresponds to a simulation based on the calculated second moment due to direct ^{113}Cd–^{113}Cd dipole–dipole interactions (eq 1b).

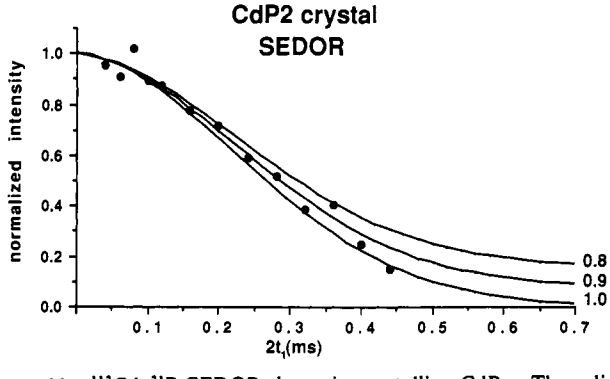

Figure 11. ^{113}Cd–^{31}P SEDOR decay in crystalline CdP_2. The solid curves correspond to simulations (eq 6) based on the calculated second moment due to direct ^{113}Cd–^{31}P dipole–dipole interactions (eq 1b) and take into account the experimentally measured ^{113}Cd spin-echo decay. Simulations have been carried out for three realistic values of a, which are indicated in the figure.

situation in CdP_2, again a comparison with the published ^{113}Cd spin-echo data on crystalline $CdAs_2$ is instructive.[34] The Cd environments in CdP_2 and $CdAs_2$ are very similar, and hence between these two compounds, the direct and indirect ^{113}Cd–^{113}Cd interactions are expected to be of comparable magnitude. In contrast, the ^{113}Cd spin-echo decays substantially faster in CdP_2. We attribute this to the partially homogeneous nature of the ^{31}P–^{31}P dipolar interaction. By using the approach by Reimer

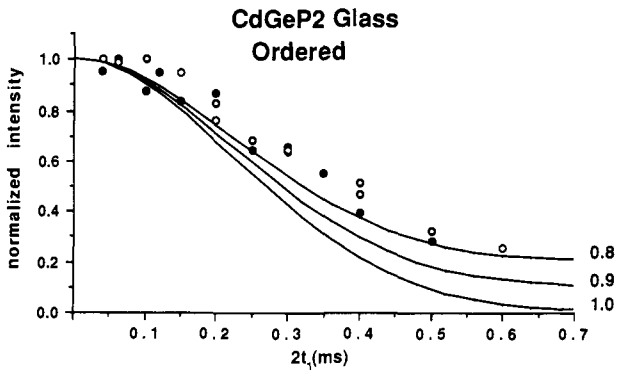

Figure 12. ^{113}Cd–^{31}P SEDOR decay in glassy $CdGeP_2$. The solid curves correspond to simulations (eq 6) based on the calculated second moment due to the direct ^{113}Cd–^{31}P dipole–dipole interactions in crystalline $CdGeP_2$ and take into account the experimentally measured ^{113}Cd spin-echo decay. Simulations have been carried out for three realistic values of a, which are indicated in the figure. Open and filled circles correspond to two independent experimental data sets.

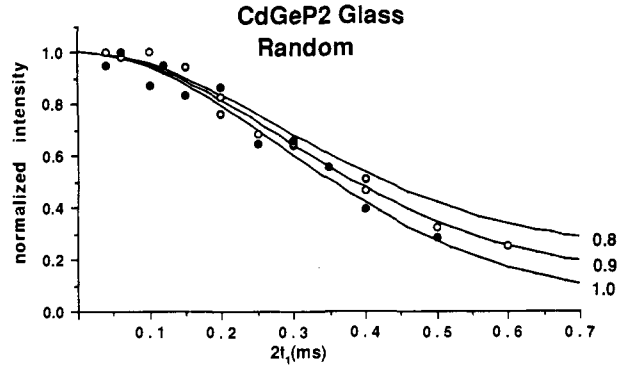

Figure 13. ^{113}Cd–^{31}P SEDOR decay in glassy $CdGeP_2$. The solid curves correspond to simulations (eq 6) based on the calculated second moment due to the direct ^{113}Cd–^{31}P dipole–dipole interactions in a lattice where both P and Cd are randomly distributed. The experimentally measured ^{113}Cd spin-echo decay is taken into account. Simulations have been carried out for three realistic values of a, which are indicated in the figure. Open and filled circles correspond to two independent experimental data sets.

and Duncan, a lower limit can be placed on $T_{2,S}$, the characteristic time constant governing these ^{31}P flip-flop processes. The analysis yields $T_{2,S}(^{31}P)_{min} = 5$ ms, if we assume that the decay in excess of the calculation from eqs 1b and 2 is exclusively due to the homogeneous character of the ^{31}P–^{31}P dipolar couplings. Larger values would result, if we assume an additional contribution arising from indirect ^{113}Cd–^{113}Cd interactions.

Although the results of the ^{31}P–^{113}Cd SEDOR experiments on CdP_2 agree reasonably well with the simulation from eqs 1b and 2, the SEDOR decay appears to be somewhat slower than expected. Reduced dipolar heteronuclear couplings have been observed previously, particularly for rare or low-γ nuclei coupled to abundant high-γ nuclei experiencing significant homonuclear interactions.[37,38] This phenomenon, termed "self-decoupling" is an unlikely explanation for the situation in CdP_2, since the ^{31}P MAS and spin-echo results indicate the ^{31}P–^{31}P flip-flop term to be moderately weak. In the present case, imperfect ^{31}P 180° pulses are the most likely reason for this discrepancy. To correct for this effect, the data need to be analyzed according to eq 6 rather than eq 5. Figure 11 includes simulations for $a = 0.9$ and 0.8, yielding improvements in the fit. Given the scatter in the data, we conclude that $a = 0.9 \pm 0.1$. Such a value is entirely realistic in view of the wide ^{31}P powder pattern (ca. 40 kHz). Since the ^{31}P wide-line spectrum of glassy $CdGeP_2$ extends over almost exactly the same frequency range, the SEDOR data on CdP_2 serve to provide our best estimate for the a value in the corresponding experiment on glassy $CdGeP_2$.

Spin Dynamics in Crystalline $CdGeP_2$. Although the second moment characterizing the ^{31}P–^{31}P interactions is substantially smaller in $CdGeP_2$ (due to the absence of P–P bonds) than in CdP_2, the small ^{31}P chemical shift anisotropy renders the ^{31}P–^{31}P dipole–dipole interactions entirely homogeneous in this case. This interaction is the main defocusing mechanism for the transverse ^{31}P magnetization in the time domain, hence precluding the formation of a spin-echo. The occurrence of ^{31}P flip-flop transitions is also clearly evident from the ^{113}Cd MAS-NMR spectra, which show dramatic line narrowing upon ^{31}P irradiation (Figure 5). Furthermore, due to the virtual absence of a ^{113}Cd chemical shift anistropy, the homogeneous character of the ^{31}P–^{31}P interaction, communicated via the ^{31}P–^{113}Cd dipolar interaction, controls the behavior of the transverse ^{113}Cd magnetization in the time domain, and thus a well-defined ^{113}Cd spin-echo is not formed. It is therefore not possible to test the spin-echo and SEDOR behavior of a hypothetical chemically ordered $CdGeP_2$ glass structure with a model compound. However, no major complications are expected in this case, provided that a large chemical shift anisotropy or dispersion is present.

Consequences for the Analysis of Glassy $CdGeP_2$ via Dipolar NMR. The experimental results presented above on CdP_2 indicate that the three dipolar NMR techniques used in the present study are not equally well suitable for the development of atomic distribution functions in glasses. This will be discussed in the paragraphs to follow.

^{31}P Spin-Echo NMR. The results shown in Figure 7 and others to be published[39] reveal that, for a wide range of crystalline phosphides and phosphorus chalcogenides, there is good agreement between experimental spin-echo decays and the simulations based on eqs 1b and 2. This good agreement validates the assumption that, over the range of evolution times of interest here ($2t_1 < 1$ ms), the refocusing of chemical shift terms by the spin-echo sequence is complete. The agreement suggests further that indirect contributions to $M_{2d}(^{31}P$–$^{31}P)$ are indeed negligible and that the ^{31}P–^{31}P dipolar coupling is predominantly heteronuclear in character. While the 20% deviation between the ^{31}P experimental and calculated second moments of CdP_2 is experimentally significant, it can be regarded as an upper limit of the error expected in the dipolar distance analysis of glassy $CdGeP_2$. Most likely, the error will be much smaller, since (a) chemical shift distribution effects will tend to quench ^{31}P flip-flop transitions in the glasses more effectively and (b) the overall strength of the ^{31}P dipolar coupling in the glasses is significantly weaker compared to CdP_2. Thus, the ^{31}P spin-echo NMR data are expected to yield fairly accurate dipolar coupling and distance information in glassy $CdGeP_2$.

^{113}Cd Spin-Echo NMR. On the basis of the experiments on CdP_2 and other model compounds, ^{113}Cd spin-echo decays are consistently more rapid than predicted by our approach, even in the absence of dipolar interactions with homogeneously coupled nuclei. Thus, it is generally not possible to neglect the effect of indirect ^{113}Cd–^{113}Cd interactions. Since the latter are not calculable from first principles, atomic distribution models derived from ^{113}Cd spin-echo decays via eq 1b are likely to be erroneous.

^{31}P–^{113}Cd SEDOR NMR. On the basis of the results presented on CdP_2, the SEDOR experiment is expected to yield reasonably accurate structural information, especially if this model compound is used to estimate the experimental correction necessary due to imperfect 180° pulses.

Structure of Glassy $CdGeP_2$. Both the ^{31}P and ^{113}Cd MAS-NMR results reveal that the local structures of glassy and crystalline $CdGeP_2$ are strikingly dissimilar. Clearly, the well-defined and highly symmetric local environments in crystalline $CdGeP_2$ are not present in the glass. The center of gravity of the ^{31}P spectrum appears to coincide with that defined by the resonances of the two inequivalent phosphorus sites in crystalline CdP_2.

(37) Abragam, A.; Winter, *Compt. Rend. Acad. Sci.* **1959**, *249*, 1633.
(38) Mehring, M.; Sinning, G.; Pines, A. *Z. Phys.* **1976**, *B24*, 73.
(39) Tepe, T.; Lathrop, D.; Franke, D.; Maxwell, R.; Banks, K.; Eckert, H. To be published.

This observation is at least consistent with the interpretation that the phosphorus environments in glassy $CdGeP_2$ are characterized by P–P bonding. A further interpretation of the observed upfield resonance displacement requires a working relationship between ^{31}P chemical shifts and structure and bonding parameters in phosphides. Although ^{31}P data have been obtained on a number of such compounds,[40-45] little is known about their structural significance. (The only serious recent attempt, made for phosphido-bridged diiron complexes,[45] is not applicable here.)

The ^{31}P spin-echo NMR results are in very good agreement with the conclusion from MAS. The spin-echo decay is substantially faster than expected for a chemically ordered structure. The comparison with simulations for crystalline $CdGeP_2$ and a random distribution of P atoms over a cubic lattice clearly illustrates that the glass structure is not chemically ordered and must contain a significant quantity of phosphorus–phosphorus bonds. (This conclusion would qualitatively remain the same even if flip-flop transitions did contribute to the dipolar broadening to a greater extent than seen in crystalline CdP_2, up to the absurd limit of a full contribution.)

Figure 8 reveals that the ^{31}P spin-echo decay data are well approximated by a 55:45 superposition of the spin-echo decays belonging to the random and the ordered model, respectively. This indicates that, although P–P bonds do occur in significant amounts, their number is clearly lower than expected for a statistical distribution of atoms. Thus, the molten state appears to retain chemical order to some extent.

If the ^{113}Cd NMR data in Figure 10 were taken at face value and the indirect interaction was neglected as well, this result would suggest that the Cd atoms are randomly distributed in the glass structure. This conclusion is questionable, however, in view of the poor agreement between experimental and calculated ^{113}Cd spin-echo decays seen with other crystalline model compounds, specifically CdP_2.

Figure 12 demonstrates clearly that the ^{113}Cd–^{31}P interaction in the glass is significantly weaker than expected in crystalline $CdGeP_2$. It is also weaker than expected, and found experimentally, in CdP_2. In both crystalline model compounds, each Cd has four Cd–P bonds. The NMR result on the glass suggests that, as a result of partial (or complete) site occupancy randomization, the average number of Cd–P bonds per Cd is significantly reduced in the glassy state. Given the fact that the best estimate for the ^{31}P inversion efficiency a (in eq 6) is 0.9 ± 0.1, the data are found to agree best with the random atomic distribution model shown in Figure 13. Although this model is the one suggested (with the reservations mentioned above) from the ^{113}Cd spin-echo data, we note that the SEDOR data only suggest that the distribution of P *relative to* Cd is random. Comparison of the SEDOR data with the 55:45 superposition of random and ordered structures yields not as good an agreement. Thus, this superposition should be viewed not as a viable structural model, but only as a heuristic approach to discuss the statistics of P–P vs P–Cd and P–Ge bonding.

The presence of pnictogen–pnictogen bonds in these glasses has been suggested previously on the basis of thermal analysis data revealing multiple recrystallization peaks of glassy $CdGeAs_2$[46] and multiple melting peaks of recrystallized $CdGeAs_2$ and $CdGeP_2$ glasses.[9] On the basis of such observations, it has been suggested that these compounds decompose partially in the molten state according to the reaction scheme $CdGeP_2 \rightarrow CdP_2 + Ge$.[9] This suggestion is compatible with the ^{31}P spin-echo decays on glassy $CdGeP_2$, if it is assumed that ca. 40% of all P atoms are present in the form of CdP_2 and 60% are present as $CdGeP_2$. On the other hand, the decomposition scheme mentioned above would preserve the basic cadmium nearest-neighbor environment (four P atoms) in contrast with the experimental results from ^{113}Cd–^{31}P SEDOR NMR. Furthermore, careful DSC studies carried out by us reveal no peak multiplicity in the crystallization of glassy $CdGeP_2$, and X-ray diffraction of the recrystallized material shows no trace of crystalline CdP_2. Thus, according to our results, this glass structure model is questionable.

Conclusions

To summarize, the results of the present study show, in four independent experiments, that glassy $CdGeP_2$ does not possess the chemically ordered structure present in the crystalline state. This result helps to rationalize the density anomaly, but contrasts sharply with the conclusion made from the previous X-ray diffraction study.[6] According to our NMR results, local ordering is essentially absent and randomization of bond formation ("chemical disorder") occurs to a large extent in these glasses, although the distribution (at least of the P atoms) is nonstatistical. The degree of chemical disordering is best quantified by ^{31}P spin-echo NMR.

It is worth pointing out that the detection of P–P bonds in glassy $CdGeP_2$ is entirely consistent with a continuous random network description of this material and in fact a necessary consequence thereof. Model building studies aimed at simulating the structure of amorphous silicon have shown that continuous random networks based on exclusively tetrahedrally bonded atoms are indeed feasible.[47] Such networks can be constructed from the diamond lattice by introducing simple bond switches,[48,49] which alter the ring statistics of the original lattice and newly introduce five- and seven-membered rings. In heteropolar structures such as the one under discussion here, such odd-membered rings imply the existence of homopolar (P–P) bonds.

The chemical disorder evident in glassy $CdGeP_2$ reveals the loss of structural integrity of this compound in the molten state. By using the NMR tools described here, it would be of interest to investigate whether the application of low-temperature methods, recently published for the synthesis of post-transition-metal phosphides,[50] could yield chemically more ordered glass structures. Such efforts would not only be a step forward toward the "structural tailoring" of such non-oxide materials for potential device applications, but also have interesting implications with regard to the question of whether chemically ordered continuous random networks based on tetrahedrally bonded atoms are at all possible.

Acknowledgment. This work has been supported by the National Science Foundation, Grant DMR 89-13738. Acknowledgment for support is also made to the Donors of the Petroleum Research Fund, administered by the American Chemical Society. We thank Ms. Kesha Banks for technical assistance.

(40) Sears, R. E. J. *Phys. Rev. B* **1978**, *18*, 3054.
(41) Duncan, T. M.; Karlicek, Jr. R. F.; Bonner, W. A.; Thiel, F. A. *J. Phys. Chem. Solids* **1984**, *45*, 389.
(42) Nissan, R. A.; Vanderah, T. A. *J. Phys. Chem. Solids* **1989**, *50*, 347.
(43) Vanderah, T. A.; Nissan, R. A. *J. Phys. Chem. Solids* **1988**, *49*, 1335.
(44) Humphries, L. R.; Sears, R. E. J. *J. Phys. Chem. Solids* **1975**, *36*, 1149.
(45) Carty, A. J.; Fyfe, C. A.; Lettinga, M.; Johnson, S.; Randall, L. H. *Inorg. Chem.* **1989**, *28*, 4120.
(46) Speyer, R. F.; Berta, Y.; Hong, K. S.; Risbud, S. H. *J. Non-Cryst. Solids* **1989**, *110*, 235.
(47) Polk, D. E. *J. Non-Cryst. Solids* **1971**, *5*, 365.
(48) Wooten, F.; Winer, K.; Weaire, D. *Phys. Rev. Lett.* **1985**, *54*, 1392.
(49) Wejchert, J.; Weaire, D.; Wooten, F. *J. Non-Cryst. Solids* **1990**, *241*, 122.
(50) Goel, S. C.; Chiang, M. Y.; Buhro, W. E. *J. Am. Chem. Soc.* **1990**, *112*, 5636.